

Decline of giant impacts on Mars by 4.48 billion years ago and an early opportunity for habitability

D. E. Moser^{1*}, G. A. Arcuri¹, D. A. Reinhard², L. F. White³, J. R. Darling⁴, I. R. Barker¹,
D. J. Larson², A. J. Irving⁵, F. M. McCubbin⁶, K. T. Tait³, J. Roszjar⁷, A. Wittmann⁸ and C. Davis¹

The timing of the wane in heavy meteorite bombardment of the inner planets is debated. Its timing determines the onset of crustal conditions consistently below the thermal and shock pressure limits for microbiota survival, and so bounds the occurrence of conditions that allow planets to be habitable. Here we determine this timing for Mars by examining the metamorphic histories of the oldest known Martian minerals, 4.476–4.429-Gyr-old zircon and baddeleyite grains in meteorites derived from the southern highlands. We use electron microscopy and atom probe tomography to show that none of these grains were exposed to the life-limiting shock pressure of 78 GPa. 97% of the grains exhibit weak-to-no shock metamorphic features and no thermal overprints from shock-induced melting. By contrast, about 80% of the studied grains from bombarded crust on Earth and the Moon show such features. The giant impact proposed to have created Mars' hemispheric dichotomy must, therefore, have taken place more than 4.48 Gyr ago, with no later cataclysmic bombardments. Considering thermal habitability models, we conclude that portions of Mars' crust reached habitable pressures and temperatures by 4.2 Gyr ago, the onset of the Martian 'wet' period, about 0.5 Gyr earlier than the earliest known record of life on Earth. Early abiogenesis by 4.2 Gyr ago, is now tenable for both planets.

The search for evidence of life on Mars continues to be a focus of planetary research, and recent work¹ heightened interest in the age range of the crust that could have hosted life. Determining the earliest time window of Martian habitability, however, requires measurements of the age at which the earliest crust transitioned permanently to a state in which both the intense shock pressures and heat (direct and indirect) caused by the early impact bombardment epoch subsided below the viability thresholds for an Earth-like deep biosphere^{2,3}. Ultimately this transition depends on the timing and rate of delivery of impact energy to the inner solar system, a poorly constrained quantity that ranges from exponential decline from the time of planet accretion at 4.56 billion years ago (Ga) and Moon formation at ~4.50 Ga (refs. 4,5) to a later pulse at 4.0–3.8 Ga due to the proposed gas giant migration, the hotly debated late heavy bombardment (LHB)⁶. Thermal habitability windows for hypothermophiles range correspondingly, from transient episodes between 4.4 and 4.1 Ga to a much later window at 3.8 Ga (ref. 3). Shock pressure waves of tens of GPa created by bombardment can also frustrate life, but experiments reveal thresholds for survival as high as 78 GPa (ref. 7) with resilience for pressure-adapted bacteria⁸. Here we present a test as to which bombardment scenario applies to early Mars by reconstructing the maximum shock pressures and temperatures experienced on Mars by zircon and baddeleyite from the oldest known Martian crust within the Rabt Sbayta Martian polymict breccia meteorites in combination with recent thermochronology⁹.

Zirconium minerals as metamorphic indicators

Zircon and baddeleyite are relatively common accessory minerals in planetary crusts and are known to faithfully record large

length-scale (hundreds of kilometres) and large-magnitude thermal and pressure perturbations that are otherwise erased in the rock record¹⁰. The microscale effects of heat (>400 °C) include resorption of crystal facets, microzircon growth and/or epitaxial overgrowths of metamorphic zircon¹¹ or, in the case of baddeleyite, rounding and truncation of igneous zoning and/or replacement by zircon¹². At the nanoscale, atom probe tomography (APT) shows that high-temperature (>800 °C) metamorphism causes clustering of trace elements, such as Pb, Al and Y (refs. 13,14). Extreme heat (>900 °C) that results from shock waves >40 GPa (ref. 15) also produces diagnostic microfeatures. In zircon, these include curvilinear fractures, partly lined with impact melt, partial-to-total conversion to granular neoblasts^{10,16} or, in impact melt sheets and ejecta blankets, the breakdown of zircon to ZrO₂ and silica¹⁷.

The micro- and nanoscale indicators of shock pressure ≥40 GPa differ for zircon and baddeleyite. Zircon microscale features include lamellae or granules of the high-pressure polymorph reidite¹⁸. Baddeleyite is more sensitive to shock pressure than most rock-forming minerals; it exhibits microscopic, orthogonally related reversion twins after shocks above 5 GPa (ref. 19) and grains at pressures >29 GPa are converted into defect-rich nanocrystalline assemblages, as seen in young Martian meteorites²⁰. At the nanoscale, the shock metamorphism of baddeleyite combined with indirect heating to ~750 °C by a kilometres-thick melt sheet caused nanoclustering of the trace elements U, Fe and Mn (ref. 21), whereas zircon at >40 GPa and 900 °C exhibits nanoclustering of Pb and Al (see below). These features can survive postimpact annealing effects that otherwise erase the shock effects in rock-forming minerals (quartz and plagioclase)¹⁰ as well as fluvial and glacial surface transport after the crater erosion²². We compared this large suite of indicators

¹Department of Earth Sciences, University of Western Ontario, London, Ontario, Canada. ²CAMECA Instruments Inc., Madison, WI, USA. ³Department of Natural History, Royal Ontario Museum, Toronto, Ontario, Canada. ⁴School of Earth and Environmental Sciences, University of Portsmouth, Portsmouth, UK. ⁵Department of Earth and Space Sciences, University of Washington, Seattle, WA, USA. ⁶NASA Johnson Space Center, Houston, TX, USA.

⁷Department of Mineralogy and Petrography, Natural History Museum Vienna, Vienna, Austria. ⁸Eyring Materials Center, Arizona State University, Tempe, AZ, USA. *e-mail: desmond.moser@uwo.ca

of pressure ≥ 5 GPa and temperatures >400 °C to the properties of individual zircon and baddeleyite grains from early Mars preserved in the meteorite North West Africa (NWA) 7034 (ref. ²³) and paired meteorites (collectively, the ‘Martian polymict breccia’ meteorites).

Meteoritic crustal fragments of early Mars

The Martian polymict breccia meteorites are recognized as a rare sample of the Martian regolith²⁴, most probably launched from Mars’ southern highlands^{24–26}, that consists of clasts of impact melt together with crystal and lithic fragments of Mars’ oldest crust^{24,27,28}. The chronology and lithological make up of these paired stones were studied by numerous groups, and some common elements in their evolution became apparent. The breccia contains diverse clasts of crystalline igneous, sedimentary and vitrophyric rocks^{24,26,29} that were assembled and welded²⁹ during a high-energy event that produced melt clasts and impact spherules with impactor components²⁴. The age of this impact event was initially estimated at ~ 1.4 Ga (refs. ^{25,29}), although recent thermochronology suggests a date as young as 0.2 Ga (ref. ⁹). Launch to Earth occurred by at least 5 million years ago (Ma) (refs. ^{9,30}). The launch event exposed the meteoroid to shock pressures between 5 and 15 GPa, which created open fractures that presently cross-cut all the components of the meteorites. These were infilled by carbonate during the residence in the Rabt Sbayta region of the Saharan desert, where the meteorites were recovered^{25,29,31}.

The oldest lithic clasts are fine-grained noritic-to-monzonitic igneous rocks and a subset of fine-grained sedimentary rocks^{25,29}. These clasts are the hosts of accessory zircon and baddeleyite, and we focus on these as they are the oldest known Martian minerals and are capable of preserving the highest-fidelity record of shock metamorphism. Two populations of crystalline zircon were recognized with ages of 4.476 ± 0.001 and 4.429 ± 0.001 Gyr (ref. ²⁸). Baddeleyite yielded U–Pb ages in the range of the younger population^{24,29}. Raman spectroscopy ($\nu_3(\text{SiO}_4)$) and photoluminescence (Dy^{3+}) of crystalline zircon ($n=10$) from NWA 7906 and NWA 7475 revealed zoning in crystallinity due to varying radiation damage (U concentration), but no evidence of zircon transformation to the high-pressure polymorph reidite³². Here we present a systematic assessment of the thermal and shock history of a larger population of zircon and baddeleyite grains to compare with those from bombarded Earth and Moon crust.

Shock metamorphic reconstructions

A total of ten polished surfaces from five paired stones (NWA 7034, NWA 7475, NWA 7906, NWA 11220 and Rabt Sbayta 003 (Supplementary Figs. 1–3) were scanned with an automated scanning electron microscopy–backscatter electron imaging–energy-dispersive spectroscopy (SEM–BSE–EDS) method (Methods). The population comprises 95 zircon and 52 baddeleyite grains (Supplementary Table 1), and 40% of the zircon and 53% of the baddeleyite occur within igneous clasts. Radiation damage in a U-rich subset of the zircon population ($n=26$, mostly crystal clasts except where in sedimentary clasts of NWA 7034²⁹) obscured the internal zoning, so these grains were not considered in our study beyond inspecting the grain outlines for signs of metamorphic forms (for example, rounding, granular neoblasts). All zircon grains in lithic clasts were found to have either the typical prismatic form (Fig. 1) or irregular forms, which ranged from euhedral to conformable with the boundaries of the host grains (Supplementary Fig. 4). Zircon crystal clasts are generally anhedral, but some retained one or two faceted surfaces. Metamorphic features were noted in the rounded form of two crystal clasts (although surface transport is another possibility for one grain) and a fractured igneous clast with possible metamorphic overgrowths ~ 300 nm wide (Supplementary Table 1). The internal microstructures of the zircon and baddeleyite populations are dominated by primary zoning, consistent with an

igneous origin. Internal zoning in crystal clasts is frequently planar and truncated at the margins, which indicates that they were parts of larger igneous grains. Many crystal clasts were probably released into the fine-grained matrix through comminution of igneous clasts during high-energy deposition of the breccia (Supplementary Figs. 4 and 5). The observations are similar for baddeleyite, as grains within rock clasts exhibit a euhedral to subhedral habit and concentric internal zoning (Supplementary Fig. 7). Crystal clasts of baddeleyite are more subhedral to anhedral, but exhibit the same internal zoning as within lithic clasts (Supplementary Fig. 9) and lithologies that represent a younger Martian crust³³.

High-resolution electron backscatter diffraction (EBSD) mapping of 69 zircon grains, which include 4.3 Ga grains²⁹, revealed two categories of lattice orientation change. Almost all grain deformations are discrete (1 – 10°) offsets across recent, open fracture sets, often conjugate, that are continuous with the launch-related fractures of the host minerals and matrix (Fig. 1 and Supplementary Figs. 4 and 5). Zircon between the fractures often exhibits low, 1 – 3° , crystal plastic deformation (Supplementary Fig. 6) that could be related to launch or a prelaunch shock event that created the coexisting spherules in the breccia. One zircon grain was found to exhibit clear prelaunch shock deformation, manifest as a set of planar deformation bands (Supplementary Fig. 11), which represent a minimum shock loading in the range 10 – 20 GPa based on Earth analogues¹⁰. These shock-induced microstructures formed on Mars as they are clearly cross-cut by, and therefore predate, launch-induced fracturing. In summary, 97% of the zircon grains exhibit a state of no-to-low (<10 GPa) shock-pressure metamorphism incurred during their time on Mars.

All 29 baddeleyite grains analysed by EBSD exhibit some combination of primary and shock-related twin domains. The primary igneous twinning is the same as that observed in terrestrial baddeleyite (that is $\{100\}$ and $\{110\}$ twins³⁴) (Supplementary Table 1). It is overprinted by micrometre to submicrometre subgrains separated by either straight, high-angle twin boundaries ($18^\circ/\{001\}$) or irregular, curved boundaries. In some grains, these discontinuous boundaries host domains with a weak diffraction. The majority of the grains ($n=26$) display three orthogonally related (90°) groupings of orientations in $\{100\}$, $\{010\}$ and $\{001\}$, as seen in the pole figures of Supplementary Figs. 8 and 10. In four grains (NWA 7475, F6396, F14987, F3590 and F3244 (Supplementary Table 1)) these relationships are defined by a small number of data (50 – 120 nm) in the EBSD map. For all orthogonally twinned grains, a single group of orientations forms 18° cross shapes. The remaining two orientation groupings are either tightly clustered ($<3^\circ$) or linearly spread and/or loosely clustered ($<10^\circ$), due to low magnitude (1 – 5°) crystal plastic deformation (for example, NWA 7475, F28444 $\{001\}$). These crystallographic features are comparable to those observed in baddeleyite exposed to shock metamorphism in the 5 – 20 GPa regime, as calibrated at the Sudbury impact structure (Canada)¹⁹. Two metamorphosed baddeleyite crystal clasts were found to exhibit replacement rims of zircon (Supplementary Figs. 12 and 13), probably due to heating and reaction with a silica-rich melt prior to emplacement in the breccia (Supplementary Fig. 12).

APT was carried out on two zircon grains and two baddeleyite grains from Mars to test for nanoscale clustering of Pb and Al as seen in high-temperature (>900 °C) shock-metamorphosed terrestrial zircon (Supplementary Fig. 14). Three microtips of a euhedral zircon grain in a lithic clast (Supplementary Fig. 5) and one microtip from a subhedral igneous zircon crystal clast (Supplementary Fig. 6) have mass spectra that match those of terrestrial reference zircon³⁵ and exhibit uniform distributions of the trace elements Al and Y (Supplementary Figs. 5 and 6). Likewise, APT analysis of euhedral baddeleyite attached to ilmenite (Supplementary Fig. 7) and a baddeleyite crystal clast (Supplementary Fig. 9) yielded mass spectra that match reference terrestrial baddeleyite³⁵ and exhibit

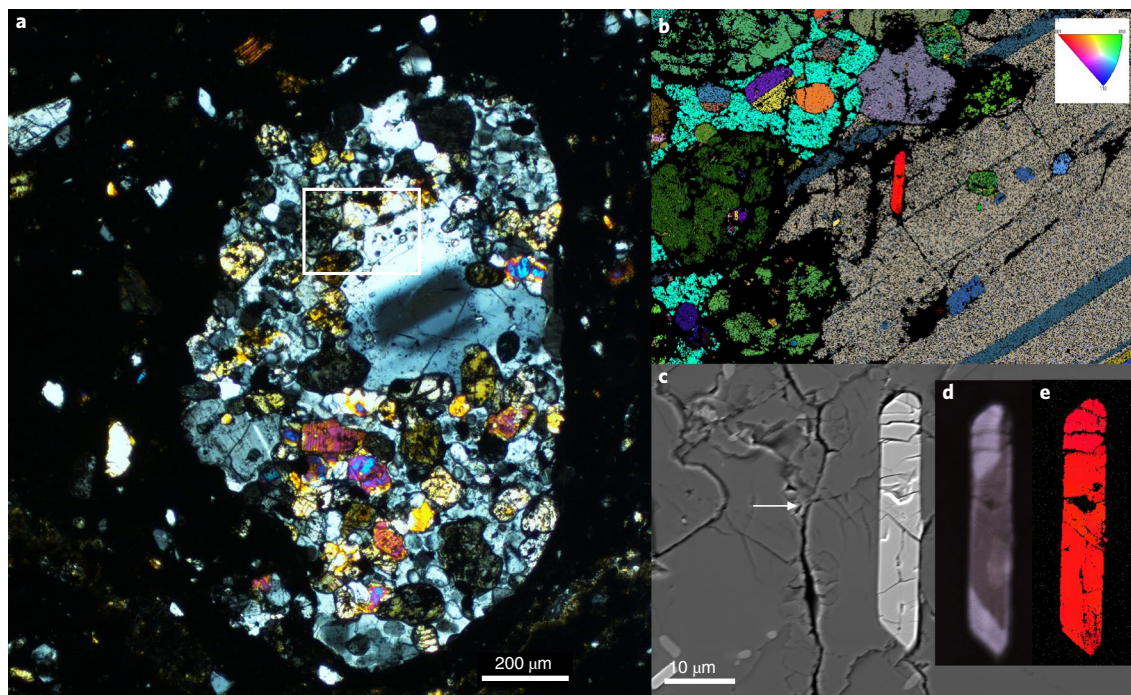


Fig. 1 | Example of early Mars crust and igneous zircon in polymict breccia meteorite NWA 11220. a, The optical micrograph shows twinned plagioclase (grey and white banding), orthopyroxene (yellow) and clinopyroxene (red/blue). **b**, The higher magnification EBSD lattice orientation map (white box in **a**) indicates highly crystalline minerals coloured according to the Euler angle relative to the sample surface, except for the zircon grain (red), coloured according to crystal axis parallel to surface. **c–e**, Highest magnification secondary electron (**c**) and cathodoluminescence (**d**) images and an EBSD orientation map (**e**) for euhedral igneous zircon that illustrates launch-related (<15 GPa (ref. ²⁵)) open fractures (white arrow). Such grains testify to the absence of major shock metamorphic effects on the source crust domain since ≥ 4.48 Ga.

Table 1 | Summary of in-situ shock microstructural analyses of zirconium minerals

| Vredefort (Earth) samples | Distance from centre of impact | Coordinates (UTM) (m) | | Total grains | % planar and/or curvilinear features | % granular features | % shock metamorphosed ^a |
|--|--------------------------------|-----------------------|-----------|--------------|--------------------------------------|---------------------|------------------------------------|
| | | East | South | | | | |
| V15-39 | ~5 km | 543,699 | 7,014,140 | 45 | 11 | 70 | 94 |
| V15-16 | ~8.6 km | 540,091 | 7,010,527 | 48 | 100 | 2 | 100 |
| V49-1 | ~8.9 km | 542,531 | 7,015,741 | 41 | 83 | 7 | 90 |
| V15-46 | ~17.1 km | 539,943 | 7,025,719 | 48 | 83 | 4 | 85 |
| V-62 | ~22.8 km | 534,627 | 7,029,025 | 33 | 91 | 15 | 97 |
| V15-55 | ~24.5 km | 563,809 | 7,030,330 | 36 | 50 | 0 | 50 |
| Overall | | | | 251 | 70 | 16 | 86 |
| Mars samples: NWA 7034, NWA 7475, NWA 7906, NWA 11220 and Rabt Sbayta 003 | | | | | | | |
| Total | | | | 121 | 1.7 | 0.8 | 2.5 |

In polished sections of bombarded crust from across the central uplift of the 2.02 Ga Vredefort impact structure compared to early Mars (>4.4 Ga) grains. The overall Earth values (zircon) are similar to the Moon results (see text). ^aShock metamorphic microstructures include planar or curvilinear features, impact-melt glass inclusions, high-pressure polymorphs (for example, reidite, zirconia and so on) or reversion products thereof, granularization or neoblastic growth and nanoscale clustering of trace elements. UTM, Universal Transverse Mercator.

homogeneous trace elemental distributions of Fe and U. These nanoscale data agree with microscale zircon and baddeleyite observations and the metamorphic state of the host minerals; all indicate predominantly low-grade (<10 GPa, <450 °C) shock- and thermal metamorphic conditions throughout the >4.43 Gyr history of the crustal terrain that sourced the igneous clasts in the breccia.

Comparison of the microstructure and Pb-loss characteristics of these grains to those from impacted crusts on the Earth and Moon show a marked difference (Table 1). Zircons from across the meta-igneous crust of the ~100 km diameter central uplift of the largest known impact on Earth, the Vredefort dome³⁶, exhibit microfeatures

of >20 GPa shock metamorphism in 87% of the grains (Table 1). Lunar zircon surveys reveal that the majority (71%) of >4 Ga grains in the Apollo impact breccias^{16,37} show such features. The opposite case is found for the Martian polymict breccia, wherein 97% of the zircons show weak-to-no shock deformation >20 GPa during the Mars residence. Likewise, the baddeleyite grains exhibit microstructures that match those in weak-to-moderately shocked domains of young Martian shergottite, but none of the features of grains near their launch-generated melt pockets²⁰. This remarkably low-intensity shock history for early Mars accessory minerals is in concert with the reported U–Pb systematics that fail to reveal

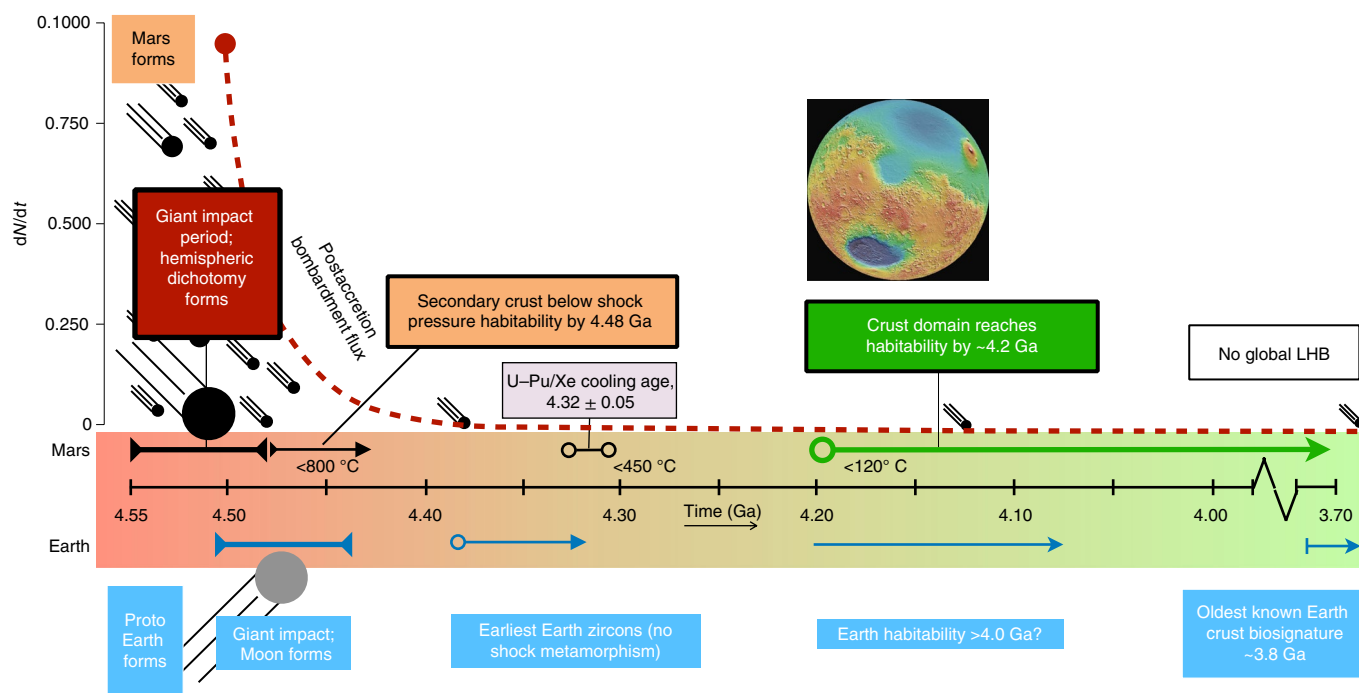


Fig. 2 | Timeline of early Mars bombardment history and habitability compared to that of Earth. The timing of major events in the early histories of Mars and Earth shows the classic postaccretion bombardment flux curve³ (red dashes) and an early period of planet-scale impact effects such as those that formed the hemispheric dichotomy, both dictated by the existence of $\leq 4.476 \pm 0.001$ Ga zircon and baddeleyite grains and host crust, unaltered by shock metamorphism >20 GPa on Mars. Note that the Mars giant impact period overlaps the current age estimates for Moon formation. The early Mars crust was below shock-pressure habitability after this time²⁸. Thermal habitability of the early Mars crust was possible at 4.4 Ga (ref. ³) and, based on the oldest U–Pu/Xe cooling date of 4.32 Ga for our samples⁹, we estimate that the source crustal terrane was habitable by 4.2 Ga, a time of accelerated volatile release after the dichotomy formation. Our samples of Mars crust did not experience a later, pervasive cataclysm at 3.9 Ga during the putative LHB⁶. Habitable crust on Mars predates Earth’s oldest known biosignatures⁵⁴ by as much as ~500 Myr. The absence of shock metamorphic features in Hadean Earth zircon¹⁵ and recent dynamical modelling⁵¹ allow that Earth also had the opportunity for early abiogenesis. Inset: the NASA-MOLA false-colour topographic model of the Mars surface (www.jpl.nasa.gov/spaceimages/details.php?id=PIA02820; Courtesy NASA/JPL-Caltech) shows the hemispheric dichotomy and southern highlands (orange), a likely source for the Martian polymict breccia meteorites^{24–26}.

impact-related Pb loss¹⁰ and instead preserve ancient, concordant (U–Pb) ages of 4.428 ± 0.025 Ga (ref. ²⁴) and up to 4.476 ± 0.001 Ga (ref. ²⁸) for zircon, and as old as 4.382 ± 0.06 Ga for baddeleyite²⁹ (Supplementary Table 4).

Early giant impact and opportunity for abiogenesis

By pairing recent chronological constraints^{9,28} with our nano- and microstructural measurements, we can refine the history of early Mars with regard to the timing of the maximum impact flux on its earliest stable crust and the time at which that crust reached habitable conditions. Recent high-precision geochronology of NWA 7034 zircon grains reveals a precursor 4.55 Ga andesitic crust on Mars that melted to crystallize a secondary crust over a 50 Myr span of igneous activity between 4.476 ± 0.001 Ga and 4.429 ± 0.001 Ga (ref. ²⁸). It is likely that the baddeleyite has a similar paragenesis, as it has an age range that is similar to zircon, is known to crystallize from mafic magmas that solidify earlier in a crustal differentiation sequence and is the dominant zirconium phase in igneous rocks from Mars³⁸. The low shock levels of most of the accessory minerals are consistent with the coexistence of primary, crystalline plagioclase in igneous clasts that host zircon (for example, as in Fig. 1) and the low shock state of rock-forming minerals in general²⁶. Exsolution lamellae in pyroxene and ilmenite in crystal and lithic clasts of the host rocks may indicate residence of the parent terrain near the surface of Mars^{25,26}, and thermochronology data indicate an upper crustal residence since 4.3 Ga (ref. ⁹). Taken together, the zircon and baddeleyite population in Martian polymict breccia meteorites and their host rocks derive from a crustal terrain that did not

experience moderate-to-high shock pressures (20–80 GPa), regional or local thermal (>450 °C) effects or Pb-loss after 4.476 ± 0.001 Ga, the age of the oldest concordant zircon²⁸. These observations provide useful brackets on the timing of giant impact and habitability on early Mars.

Calculations of heat thresholds for early life during bombardment relate to the energy release of impactors, and an impactor diameter of 500 km is sufficient to eliminate survivable conditions for deep thermophiles on Mars and Earth³⁹. An impactor as large as the size of 1 Ceres (~1,000 km diameter) is proposed to have struck early Mars to create its distinctive hemispheric crustal dichotomy in thickness and topography⁴⁰, and must have had profound shock pressure and thermal consequences for crustal minerals at all scales. We can place the time interval for the planet-shaping impactor collision at 4.51 ± 0.04 Ga based on the upper bracket of 4.55 Ga for first crust formation²⁸ and a lower bracket based on the weak shock and thermal metamorphic history of our samples of the secondary crust and its oldest concordant zircon age of 4.476 ± 0.001 Ga (ref. ²⁸) (Fig. 2). This agrees with the minimum age bracket of 4.42 ± 0.07 Ga for the dichotomy formation derived from Sm–Nd geochronology⁴¹, for which, however, it was impossible to distinguish the cause for the dichotomy as due to mantle overturn or giant impact⁹. Recent Lu–Hf chronological constraints show that mantle overturn was complete within 20 Myr of planet formation²⁸ and thus falsify an endogenous origin for the dichotomy due to 1° (that is, whole) mantle overturn, as the latter requires >100 Myr to actuate⁴². It is possible that the zircon and baddeleyite crystallization events between 4.476 ± 0.001 Ga and 4.429 ± 0.001 Ga (ref. ²⁸) represent a

long period of crystallization after the global melting of primary crust by the giant impact (Fig. 2) in view of the high impactor content of the igneous clasts²⁴.

This early, 4.51 ± 0.04 Ga age for the formation of the hemispheric dichotomy aligns with the period of Moon formation^{4,5}, and is a maximum age for habitability conditions (Fig. 2). In fact, it establishes the start of the very early time period for which volatiles, which include water and organic compounds, could have been liberated and accumulated at the surface and in the near subsurface through volcanic processes^{43,44} after a giant impact. A global equivalent layer of water in the range of 229 m is thought to have been present at the Martian surface early in its history through such volcanic degassing⁴⁵, which is sufficient to account for some of the early water-related geomorphic features and may support the former presence of shallow seas. Our shock-pressure reconstruction for this period indicates the existence of a weakly shocked crustal terrain that, in regard to pressure, was habitable from the beginning. The main threat from shock pressure to microorganisms in the early crustal terrains is the mechanical shearing effects on cell walls⁴⁶; however, such effects are well-known to be highly heterogeneous at the microscale¹⁵. Moreover, the terrain did not experience shock pressures >15 GPa, which is well below the known upper limit of viability of 78 GPa (ref. 7).

It appears, therefore, that temperature, rather than shock pressure, was the more important of the two factors to limit the onset of habitability of the early Mars crust. The two are tightly linked during the bombardment period and have been modelled with respect to crustal habitability volumes relative to the early versus late timing of the peak impactor flux³. Our mineral evidence supports the classic postaccretion model³ of peak bombardment beginning at 4.57 Ga (ref. 47) with a monotonic decline that caused local impact effects (for example, as in our few shocked grains (Supplementary Table 1)), relict terrains unmodified by intense metamorphism and crust viable for hyperthermophiles down to 8 km as early as 4.4 Ga. This is in line with U–Pu/Xe gas thermochronology results for whole-rock samples of NWA 7034 that yielded cooling as early as 4.319 ± 0.046 Ga below temperatures of at least ~ 450 °C based on a comparison with Pb behaviour in coexisting phosphates⁹. For the Rabt Sbayta polymict breccia, we place a conservative age estimate of 4.2 Ga for the time at which the crustal fragments cooled to the thermal habitability window of ~ 120 °C, based on modelled rates of crustal thermal decay after postaccretion bombardment³ (Fig. 2). We note that there is no evidence that our sample of the southern highlands of Mars suffered a later global, thermal or structural modification of the crust and hydrosphere by the putative 4.0–3.8 Ga LHB². For the Earth, the LHB is predicted to have been thermally cataclysmic for life, melting the outer crust down to 10 km, due to the cumulative effects of impact-triggered surface melting and pressure-release melting from the early mantle⁴⁸ (Fig. 2). Indeed, if such an event occurred, its effects were not pervasive on Mars. This is consistent with dynamic modelling⁴⁹ and isotopic evidence⁵⁰, which proposes either that Mars escaped an LHB or, our favoured hypothesis, that gas giant planet migration occurred within the first 100 Myr of accretion⁵¹ such that an LHB did not take place.

The time window for abiogenesis on Mars could have been as long as 700 Myr, from 4.2 to 3.5 Ga, based on evidence that the Martian surface became much less hospitable by approximately 3.5 Ga (refs. 52,53). This 700 Myr period is longer than Earth's Phanerozoic eon, and more than the amount of time between accretion and the first signs of life on Earth at ~ 3.8 Ga (ref. 54). Based on terrestrial geology, Mars' crust could predate the oldest known inhabited surface of Earth by half a billion years (Fig. 2). Alternatively, based on recent dynamic models⁵¹, it is plausible that Earth, like Mars, experienced major bombardment only in the first ~ 100 Myr, and likewise exhibited early habitable crustal platforms. Ar–Ar geochronology and cosmogenic nuclide exposure histories suggest that the earliest

Mars crust fragments derived from a terrain of hundreds of square kilometres that remained near the present surface⁹ as opposed to being deeply buried by later volcanism²⁸. It is possible that this rock record of earliest habitability remains accessible in the modern Martian crust and pertinent to future mission planning for sample return.

Online content

Any methods, additional references, Nature Research reporting summaries, source data, statements of code and data availability and associated accession codes are available at <https://doi.org/10.1038/s41561-019-0380-0>.

Received: 12 September 2018; Accepted: 1 May 2019;

Published online: 24 June 2019

References

- Eigenbrode, J. L. et al. Organic matter preserved in 3-billion-year-old mudstones at Gale crater, Mars. *Science* **360**, 1096–1101 (2018).
- Ryder, G. Mass flux in the ancient Earth–Moon system and benign implications for the origin of life on Earth. *J. Geophys. Res.* **107**, 5022 (2002).
- Abramov, O. & Mojzsis, S. J. Thermal effects of impact bombardments on Noachian Mars. *Earth Planet. Sci. Lett.* **442**, 108–120 (2016).
- Touboul, M., Kleine, T., Bourdon, B., Palme, H. & Wieler, R. Late formation and prolonged differentiation of the Moon inferred from W isotopes in lunar metals. *Nature* **450**, 1206–1209 (2007).
- Barboni, M. et al. Early formation of the Moon 4.51 billion years ago. *Sci. Adv.* **3**, e1602365 (2017).
- Gomes, R., Levison, H. F., Tsiganis, K. & Morbidelli, A. Origin of the cataclysmic late heavy bombardment period of the terrestrial planets. *Nature* **435**, 466–469 (2005).
- Hazael, R., Meersman, F., Ono, F. & McMillan, P. F. Pressure as a limiting factor for life. *Life* **6**, 34 (2016).
- Hazael, R., Fitzmaurice, B. C., Foglia, F., Appleby-Thomas, G. J. & McMillan, P. F. Bacterial survival following shock compression in the gigapascal range. *Icarus* **293**, 1–7 (2017).
- Cassata, W. S. et al. Chronology of Martian breccia NWA 7034 and the formation of the Martian crustal dichotomy. *Sci. Adv.* **4**, eaap8306 (2018).
- Moser, D. E. et al. New zircon shock phenomena and their use for dating and reconstruction of large impact structures revealed by electron nanobeam (EBSD, CL, EDS) and isotopic U–Pb and (U–Th)/He analysis of the Vredefort dome. *Can. J. Earth Sci.* **48**, 117–139 (2011).
- Kohn, M. J. & Kelly, N. M. in *Microstructural Geochronology: Planetary Records Down to Atom Scale* (eds Moser, D. E. et al.) 35–61 (Wiley, 2017).
- Heaman, L. M. & LeCheminant, A. N. Paragenesis and U–Pb systematics of baddeleyite (ZrO₂). *Chem. Geol.* **110**, 95–126 (1993).
- Valley, J. W. et al. Hadean age for a post-magma-ocean zircon confirmed by atom-probe tomography. *Nat. Geosci.* **7**, 219–223 (2014).
- Piazolo, S. et al. Deformation-induced trace element redistribution in zircon revealed using atom probe tomography. *Nat. Commun.* **7**, 10490 (2016).
- Stöfler, D., Hamann, C. & Metzler, K. Shock metamorphism of planetary silicate rocks and sediments: proposal for an updated classification system. *Meteorit. Planet. Sci.* **53**, 5–49 (2018).
- Crow, C. A., Moser, D. E. & McKeegan, K. D. Shock metamorphic history of >4 Ga Apollo 14 and 15 zircons. *Meteorit. Planet. Sci.* **54**, 181–201 (2019).
- El Goresy, A. Baddeleyite and its significance in impact glasses. *J. Geophys. Res.* **70**, 3453–3456 (1965).
- Erickson, T. M. et al. Microstructural constraints on the mechanisms of the transformation to reidite in naturally shocked zircon. *Contrib. Mineral. Petrol.* **172**, 6 (2017).
- White, L. F. et al. Baddeleyite as a widespread and sensitive indicator of meteorite bombardment in planetary crusts. *Geology* **46**, 719–722 (2018).
- Darling, J. R. et al. Variable microstructural response of baddeleyite to shock metamorphism in young basaltic shergottite NWA 5298 and improved U–Pb dating of Solar System events. *Earth Planet. Sci. Lett.* **444**, 1–12 (2016).
- White, L. F. et al. Atomic-scale age resolution of planetary events. *Nat. Commun.* **8**, 15597 (2017).
- Thomson, O. A. et al. Preservation of detrital shocked minerals derived from the 1.85 Ga Sudbury impact structure in modern alluvium and Holocene glacial deposits. *Bull. Geol. Soc. Am.* **126**, 720–737 (2014).
- Agee, C. B. et al. Unique meteorite from early Amazonian Mars: water-rich basaltic breccia Northwest Africa 7034. *Science* **339**, 780–785 (2013).
- Humayun, M. et al. Origin and age of the earliest Martian crust from meteorite NWA 7533. *Nature* **503**, 513–516 (2013).
- Wittmann, A. et al. Petrography and composition of Martian regolith breccia meteorite Northwest Africa 7475. *Meteorit. Planet. Sci.* **50**, 326–352 (2015).

26. Hewins, R. H. et al. Regolith breccia Northwest Africa 7533: mineralogy and petrology with implications for early Mars. *Meteorit. Planet. Sci.* **52**, 89–124 (2017).
27. Bellucci, J. J. et al. A scanning ion imaging investigation into the micron-scale U–Pb systematics in a complex lunar zircon. *Chem. Geol.* **438**, 112–122 (2016).
28. Bouvier, L. C. et al. Evidence for extremely rapid magma ocean crystallization and crust formation on Mars. *Nature* **558**, 586–589 (2018).
29. McCubbin, F. M. et al. Geologic history of Martian regolith breccia Northwest Africa 7034: evidence for hydrothermal activity and lithologic diversity in the Martian crust. *J. Geophys. Res. Planets* **121**, 2120–2149 (2016).
30. Cartwright, J. A., Ott, U., Herrmann, S. & Agee, C. B. Modern atmospheric signatures in 4.4 Ga Martian meteorite NWA 7034. *Earth Planet. Sci. Lett.* **400**, 77–87 (2014).
31. Lorand, J. P. et al. Nickeliferous pyrite tracks pervasive hydrothermal alteration in Martian regolith breccia: a study in NWA 7533. *Meteorit. Planet. Sci.* **50**, 2099–2120 (2015).
32. Roszjar, J., Moser, D. E., Hyde, B. C., Chanmuang, C. & Tait, K. in *Microstructural Geochronology: Planetary Records Down to Atom Scale* (eds Moser, D. E. et al.) 113–135 (Wiley, 2017).
33. Moser, D. E. et al. Solving the Martian meteorite age conundrum using micro-baddeleyite and launch-generated zircon. *Nature* **499**, 454–457 (2013).
34. Wingate, M. T. D. & Compston, W. Crystal orientation effects during ion microprobe U–Pb analysis of baddeleyite. *Chem. Geol.* **168**, 75–97 (2000).
35. Reinhard, D. A. et al. in *Microstructural Geochronology: Planetary Records Down to Atom Scale* (eds Moser, D. E. et al.) 315–326 (Wiley, 2017).
36. Therrault, A. M., Grieve, R. A. F. & Reimold, W. U. Original size of the Vredefort structure: implications for the geological evolution of the Witwatersrand Basin. *Meteorit. Planet. Sci.* **32**, 71–77 (1997).
37. Crow, C. A., McKeegan, K. D. & Moser, D. E. Coordinated U–Pb geochronology, trace element, Ti-in-zircon thermometry and microstructural analysis of Apollo zircons. *Geochim. Cosmochim. Acta* **202**, 264–284 (2017).
38. Herd, C. D. K. et al. in *Microstructural Geochronology: Planetary Records Down to Atom Scale* (eds Moser, D. E. et al.) 137–166 (Wiley, 2017).
39. Sleep, N. H. & Zahnle, K. Refugia from asteroid impacts on early Mars and the early Earth. *J. Geophys. Res.* **103**, 28529–28544 (1998).
40. Wilhelms, D. E. & Squyres, S. W. The Martian hemispheric dichotomy may be due to a giant impact. *Nature* **309**, 138–140 (1984).
41. Nyquist, L. E. et al. Rb–Sr and Sm–Nd isotopic and REE studies of igneous components in the bulk matrix domain of Martian breccia Northwest Africa 7034. *Meteorit. Planet. Sci.* **51**, 483–498 (2016).
42. Watters, T. R., McGovern, P. J. & Irwin, R. P. III Hemispheres apart: the crustal dichotomy on Mars. *Annu. Rev. Earth Planet. Sci.* **35**, 621–652 (2007).
43. Steele, A. et al. A reduced organic carbon component in Martian basalts. *Science* **337**, 212–215 (2012).
44. Carr, M. H. & Head, J. W. Martian surface/near-surface water inventory: sources, sinks, and changes with time. *Geophys. Res. Lett.* **42**, 726–732 (2015).
45. McCubbin, F. M. et al. Heterogeneous distribution of H₂O in the Martian interior: implications for the abundance of H₂O in depleted and enriched mantle sources. *Meteorit. Planet. Sci.* **51**, 2036–2060 (2016).
46. Horneck, G. et al. Microbial rock inhabitants survive hypervelocity impacts on Mars-like host planets: first phase of lithopanspermia experimentally tested. *Astrobiology* **8**, 17–44 (2008).
47. Bottke, W. F. & Andrews-Hanna, J. C. A post-accretionary lull in large impacts on early Mars. *Nat. Geosci.* **10**, 344–348 (2017).
48. Marchi, S. et al. Widespread mixing and burial of Earth's Hadean crust by asteroid impacts. *Nature* **511**, 578–582 (2014).
49. Brasser, R., Mojzsis, S. J., Werner, S. C., Matsumura, S. & Ida, S. Late veneer and late accretion to the terrestrial planets. *Earth Planet. Sci. Lett.* **455**, 85–93 (2016).
50. Dauphas, N. & Pourmand, A. Hf–W–Th evidence for rapid growth of Mars and its status as a planetary embryo. *Nature* **473**, 489–492 (2011).
51. Nesvorný, D., Vokrouhlický, D., Bottke, W. F. & Levison, H. F. Evidence for very early migration of the Solar System planets from the Patroclus–Menoetius binary Jupiter Trojan. *Nat. Astron.* **2**, 878–882 (2018).
52. Hurowitz, J. A. & McLennan, S. M. A ~3.5 Ga record of water-limited, acidic weathering conditions on Mars. *Earth Planet. Sci. Lett.* **260**, 432–443 (2007).
53. Ehlmann, B. L. et al. The sustainability of habitability on terrestrial planets: insights, questions, and needed measurements from Mars for understanding the evolution of Earth-like worlds. *J. Geophys. Res. Planets* **121**, 1927–1961 (2016).
54. Rosing, M. T. ¹³C-depleted carbon microparticles in >3700-Ma sea-floor sedimentary rocks from West Greenland. *Science* **283**, 674–676 (1999).

Acknowledgements

The following curators and institutions are acknowledged for providing sample material; B. Hofmann (Naturhistorisches Museum Bern) for the loan of NWA 7906, J. Kashuba for the loan of the NWA 11220 thin sections and B. Hoefnagels for the loan of Rabt Sbayta 003. The following are acknowledged for their assistance with making or running the APT specimens: T. J. Prosa, I. Martin, K. P. Rice, Y. Chen, D. Olson and D. Lawrence. W. U. Reimold and R. Hewins are thanked for their thoughtful reviews. Graphics assistance from K. Vankerkoerle is acknowledged. D.E.M. acknowledges support for electron microscopy analyses, student and technical scientist funding, and facility travel costs from his NSERC Discovery Grant; J.R.D. acknowledges support from Royal Society Research Grant RG160237 and a University of Portsmouth RIEF award; F.M.M. acknowledges support from NASA's Planetary Science Research Program; K.T.T. acknowledges NSERC Discovery Grant support.

Author contributions

D.E.M. was in charge of the conceptualization of the project and writing the initial draft. All the authors provided support in one or more of the roles of investigation, formal analysis, resource provision and written contributions to subsequent drafts of the manuscript. A.J.I. was the classifier of two of the specimens used in this study and provided thin and thick sections for detailed analyses.

Competing interests

We note that the CAMECA co-authors (D.A.R. and D.J.L.) are engaged in the manufacture and sale of atom probe instruments. The remaining authors declare no competing interests.

Additional information

Supplementary information is available for this paper at <https://doi.org/10.1038/s41561-019-0380-0>.

Reprints and permissions information is available at www.nature.com/reprints.

Correspondence and requests for materials should be addressed to D.E.M.

Publisher's note: Springer Nature remains neutral with regard to jurisdictional claims in published maps and institutional affiliations.

© The Author(s), under exclusive licence to Springer Nature Limited 2019

Methods

Electron microscopy. Petrographic slabs and thick and thin sections were created from the collected samples using standard sample preparation techniques²⁹. The sections were subjected to a final polishing step using a colloidal silica solution (0.05 µm, pH 8.5) and a vibratory polisher. Electron microscopy was performed with a Hitachi SU6600 field-emission SEM (Schottky emitter) located in the Zircon and Accessory Phase Laboratory at the University of Western Ontario. Features of interest (for example, zircon and baddeleyite) were initially located using BSE imaging (five segment solid-state detector) and EDS (Oxford X-max 80 mm² silicon drift detector) within Oxford INCA's Feature mapping routine, at an accelerating voltage of 15 kV (ref. ¹⁰); these features were subsequently overlain on BSE and/or EDS section montages by plotting the feature's stage coordinates using Esri's ArcGIS.

Automated SEM–BSE–EDS mapping was used to identify target grain locations and dimensions prior to characterizing the micro- and nanoscale features. Many hundreds of grains, mostly in the 1 µm to 9 µm size range, were detected and are mostly angular fragments in the breccia matrix. The size fraction larger than 10 µm in maximum dimension ($n = 147$) (Supplementary Table 1) was examined using electron microscopy, which included secondary electrons, backscattered electrons, cathodoluminescence and EBSD, to determine the internal zoning patterns, lattice orientation microstructure, crystallinity and any metamorphic polymorphs (for example, reidite) or phase-transition heritage. There was no directional fabric in the grain populations, and hence the analysed surfaces include random intersections of larger (>50 µm) grains, such as those liberated by crushing²⁸ and shown on some surfaces (for example, Supplementary Fig. 4).

Each crystalline grain ($n = 121$ for the Martian samples) was examined using BSE and/or cathodoluminescence for microscopic primary features, secondary metamorphic features¹¹ and the suite of shock metamorphic indicators described above. The largest (by length) features of each sample were extensively imaged using secondary electron, BSE and EDS point analysis to capture the morphology and associated phases. Several of these grains were then analysed further using other methods, including EDS mapping, cathodoluminescence and EBSD. Colour cathodoluminescence images were collected for all but NWA 7906 with a customized Gatan ChromaCL red–green–blue (RGB) plus ultraviolet detector system and Gatan Digital Micrograph software using a 10 kV electron beam and 250 µs pixel time. Microstructural EBSD orientation data were captured with an Oxford Nordlys detector and HKL's Channel5 software. Samples were tilted to 70° within the SEM chamber and raised to a working distance of 19.0 mm. Kikuchi patterns were generated using a 20 kV, 8.0 nA electron beam, and captured using the camera settings of 24 ms/frame acquisition time, 4 × 4 pixel binning, high gain and frame averaging of seven. Patterns were then indexed using a minimum of five and a maximum of seven Kikuchi bands, and a Hough transform resolution setting of 60. Beam step sizes during the mapping were 60 nm to 125 nm, but most commonly 125 nm. A mean angular deviation discriminator was set to a value of 1.5, above which analyses were assigned a zero solution to avoid the indexing of poor-quality EBS patterns. Postanalysis noise-reduction processing was not applied to any of the data sets other than to remove erroneous 'wild spikes'. Orientation microstructure and crystallographic analysis by EBSD was used to evaluate pre- and postlaunch shock-induced microstructures and search for signs of high-pressure polymorphs or their reversion products. The same instruments and procedures were used for the shock microstructural survey of zircons in petrographic thin sections across the Vredefort impact structure (Table 1), as detailed in the source MSc thesis by C. Davis (<https://ir.lib.uwo.ca/etd/4185/>)⁵⁵. NWA 7906 was analysed at the Natural History Museum Vienna. Cathodoluminescence images were obtained using a Gatan MonoCL (MonoCL4R) system attached to a JEOL JSM 6610-LV SEM. Monochromatic images were obtained by using a wavelength-filtered (monochromatic) RGB setting that yielded false-colour (composite) RGB images, while panchromatic (greyscale) images

resulted from the integration of the luminescence over all emissions. Operating conditions for all SEM-MonoCL images were a 15 kV accelerating voltage, a 1.2 nA beam current and a working distance of ~11 mm (ref. ³²).

APT. APT allows the three-dimensional mapping and identification of elements and isotopes within minerals¹³. APT data sets were prepared by gallium-focused ion beam milling at CAMECA Instruments Inc. Standard liftoff and mount techniques were used to produce the desired specimen shape with a radius of curvature <100 nm (refs. ^{36,37}). A final low voltage (10 kV) milling step was performed to help minimize the gallium implantation and damage. Prepared microtips were analysed at CAMECA using a LEAP 4000X HR atom probe equipped with a reflectron flight path and operated in the laser pulsed mode. Field evaporation of each microtip was induced under an ultrahigh vacuum by applying a high electric field (achieved with 4–12 kV) at cryogenic conditions (~50–60 K) to the specimen apex. In the laser pulse mode, ionization and evaporation of the atoms on the specimen surface was promoted by an ultraviolet laser (355 nm wavelength) with pulse energies and frequencies that varied between ~100 and 400 pJ and ~150 and 200 kHz, respectively. During acquisition, the mass-to-charge ratio of the ions was determined through time-of-flight mass spectrometry by measuring the time from field evaporation to detection and equating it to their kinetic energy. A spatial reconstruction of the specimen was achieved by projecting the ions from a position-sensitive detector back to the tip apex and considering the sequential order of evaporation. Full details of the data acquisition and reconstruction with the local electrode atom probe are described elsewhere⁵⁸.

Data analysis and the ranging of mass spectra were conducted using the CAMECA IVAS 3.6.12 software. For each microtip data set, the corrected ionic counts of major and trace elements were calculated through the subtraction of background counts from the raw ionic counts. The background counts were measured using the local range-assisted background model in IVAS. In all scenarios, the peak locations of the trace element (for example, Y, Fe, Al, U and Pb) were identified within each microtip spectrum using the BR266 zircon standard and the baddeleyite standard Phalaborwa as reference materials³⁵. For individual peaks, range bounds were set by eye from baseline to baseline to encompass the entirety of the visible portion of each peak²¹. Note, however, that there are no standard protocols with which to set range widths, and it is a key source of variation that is actively being explored in the field (for example, Larson et al.⁵⁸ and Blum et al.⁵⁹). Details on the acquisition and spatial reconstruction parameters selected for this work are given in Supplementary Table 3.

Data availability

All the data are summarized and available in the main text or the Supplementary Information. Raw instrument data are available to editors and reviewers upon request.

References

- Davis, C. L. *Microstructural Geochronology of Zircon across the Central Uplift of the Vredefort Impact Structure, South Africa* MSc thesis, University of Western Ontario (2017).
- Larson, D. J. et al. Field-ion specimen preparation using focused ion-beam milling. *Ultramicroscopy* **79**, 287–293 (1999).
- Thompson, K. et al. In situ site-specific specimen preparation for atom probe tomography. *Ultramicroscopy* **107**, 131–139 (2007).
- Larson, D. J., Prosa, T. J., Ulfig, R. M., Geiser, B. P. & Kelly, T. F. *Local Electrode Atom Probe Tomography* (Springer, 2013).
- Blum, T. B. et al. in *Microstructural Geochronology: Planetary Records Down to Atom Scale* (eds Moser, D. E. et al.) 237–350 (Wiley, 2017).